Report

Current Biology

Visual-Olfactory Integration in the Human Disease Vector Mosquito *Aedes aegypti*

Graphical Abstract

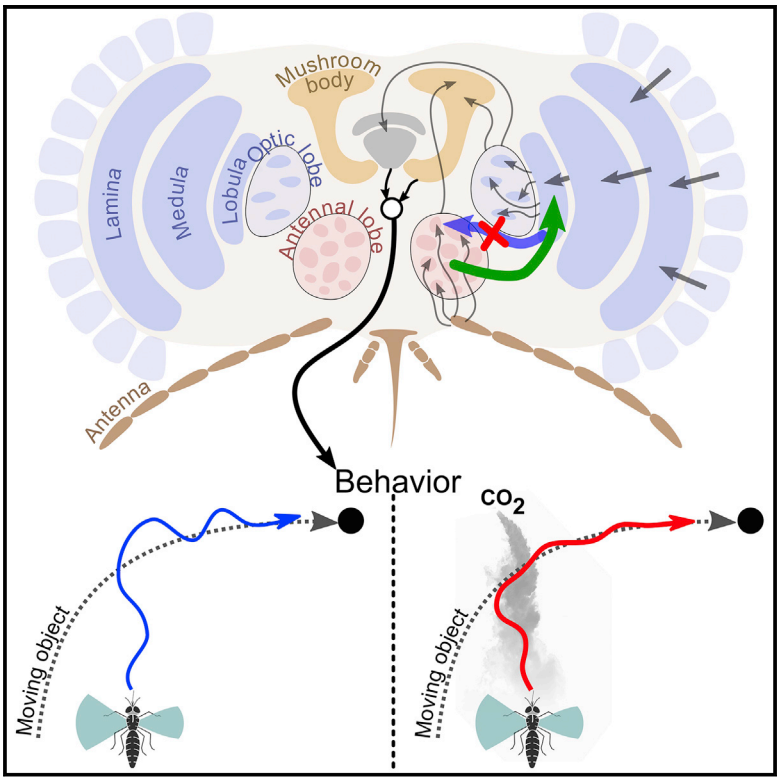

Authors

Clément Vinauger, Floris Van Breugel, Lauren T. Locke, ..., Adrienne L. Fairhall, Omar S. Akbari, Jeffrey A. Riffell

Correspondence

jriffell@uw.edu

In Brief

When mosquitoes encounter CO_2, they become attracted to dark, visual objects. Using tethered mosquitoes and calcium imaging experiments, Vinauger, Van Breugel et al. find that CO_2 modulates lobula neuropil responses to discrete visual stimuli. This modulation may facilitate host tracking by navigating mosquitoes.

Highlights

- CO_2 modulates mosquito behavioral responses to discrete visual stimuli
- CO_2 modulates lobula neuropil responses to discrete visual stimuli
- Visual stimuli do not modulate responses to CO_2 in olfactory glomeruli
- Modulation of peripheral visual and olfactory sensory stimuli is asymmetric

Vinauger et al., 2019, Current Biology *29*, 1–8
August 5, 2019
https://doi.org/10.1016/j.cub.2019.06.043

CellPress

Please cite this article in press as: Vinauger et al., Visual-Olfactory Integration in the Human Disease Vector Mosquito *Aedes aegypti*, Current Biology (2019), https://doi.org/10.1016/j.cub.2019.06.043

Current Biology
Report

Visual-Olfactory Integration in the Human Disease Vector Mosquito *Aedes aegypti*

Clément Vinauger,[1,7] Floris Van Breugel,[2,7] Lauren T. Locke,[3] Kennedy K.S. Tobin,[3] Michael H. Dickinson,[4] Adrienne L. Fairhall,[5] Omar S. Akbari,[6] and Jeffrey A. Riffell[3,8,*]
[1]Department of Biochemistry, Virginia Polytechnic Institute and State University, Blacksburg, VA 24061, USA
[2]Department of Mechanical Engineering, University of Nevada-Reno, Reno, NV 89557, USA
[3]Department of Biology, University of Washington, Seattle, WA 98195, USA
[4]Division of Biology and Biological Engineering, California Institute of Technology, Pasadena, CA 91125, USA
[5]Department of Physiology and Biophysics, University of Washington, Seattle, WA 98195, USA
[6]Section of Cell and Developmental Biology, University of California, San Diego, San Diego, CA 92093, USA
[7]These authors contributed equally
[8]Lead Contact
*Correspondence: jriffell@uw.edu
https://doi.org/10.1016/j.cub.2019.06.043

SUMMARY

Mosquitoes rely on the integration of multiple sensory cues, including olfactory, visual, and thermal stimuli, to detect, identify, and locate their hosts [1–4]. Although we increasingly know more about the role of chemosensory behaviors in mediating mosquito-host interactions [1], the role of visual cues is comparatively less studied [3], and how the combination of olfactory and visual information is integrated in the mosquito brain remains unknown. In the present study, we used a tethered-flight light-emitting diode (LED) arena, which allowed for quantitative control over the stimuli, and a control theoretic model to show that CO_2 modulates mosquito steering responses toward vertical bars. To gain insight into the neural basis of this olfactory and visual coupling, we conducted two-photon microscopy experiments in a new GCaMP6s-expressing mosquito line. Imaging revealed that neuropil regions within the lobula exhibited strong responses to objects, such as a bar, but showed little response to a large-field motion. Approximately 20% of the lobula neuropil we imaged were modulated when CO_2 preceded the presentation of a moving bar. By contrast, responses in the antennal (olfactory) lobe were not modulated by visual stimuli presented before or after an olfactory stimulus. Together, our results suggest that asymmetric coupling between these sensory systems provides enhanced steering responses to discrete objects.

RESULTS AND DISCUSSION

Many animals integrate different sensory modalities to make robust behavioral decisions. For example, in bees and humans, prior exposure to a visual stimulus can modify olfactory responses [5–7] and vice versa [8]. To detect and locate suitable hosts, mosquitoes rely on multiple sensory cues, including olfactory, visual, and thermosensory information [1–4, 9], while flying through a dynamic environment [10]. Whereas mosquitoes' responses to olfactory [11–13] and thermal stimuli [14, 15] have been well studied, comparatively less is known about their visually mediated behaviors (but see [16, 17]). A recent study with freely flying mosquitoes showed that CO_2 detection activates a strong attraction to visual features that is critical for mediating interaction with close-range cues, such as heat, and other host volatiles [3]. How the visual and olfactory signals are integrated in the brain, however, remains an open question.

Here, to study the integration of multimodal host signals in *Ae. aegypti*, we placed tethered, mated females within a cylindrical light-emitting diode (LED) arena [18] that permitted simultaneous presentation of olfactory stimuli with the motion of high-contrast visual objects in a controlled manner (Figure 1A). We monitored the mosquitoes' responses to visual and olfactory cues by tracking changes in wingbeat frequency and stroke amplitude of their left and right wings; proxies for acceleration and turning behavior. After establishing behavioral evidence of visual-olfactory integration in this tethered preparation, we used two-photon calcium imaging to investigate the neural basis for this integration.

Tethered Mosquitoes Increase Their Wingbeat Frequency and Amplitude in Response to CO_2

Our first step was to characterize tethered mosquitoes' behavioral responses to host cues. We placed the animals in a static visual environment composed of multiple dark vertical bars (22.5° wide × 54° tall, spaced by 22.5°) and presented them with pulses of CO_2, a key attractant for host localization [20]. To characterize the behavioral response to CO_2, we measured changes in wingbeat frequency (WBF) and the sum and difference in wingbeat amplitude (L+R WBA and L−R WBA) (Figure 1B). In free flight, insects, including mosquitoes, exhibit an upwind surge behavior when they encounter an attractive odor [19, 21–24]; in the tethered preparation, this surge is manifested by increases in WBF and L+R WBA. Increases in the absolute value of L−R WBA, on the other hand, are correlated with turning

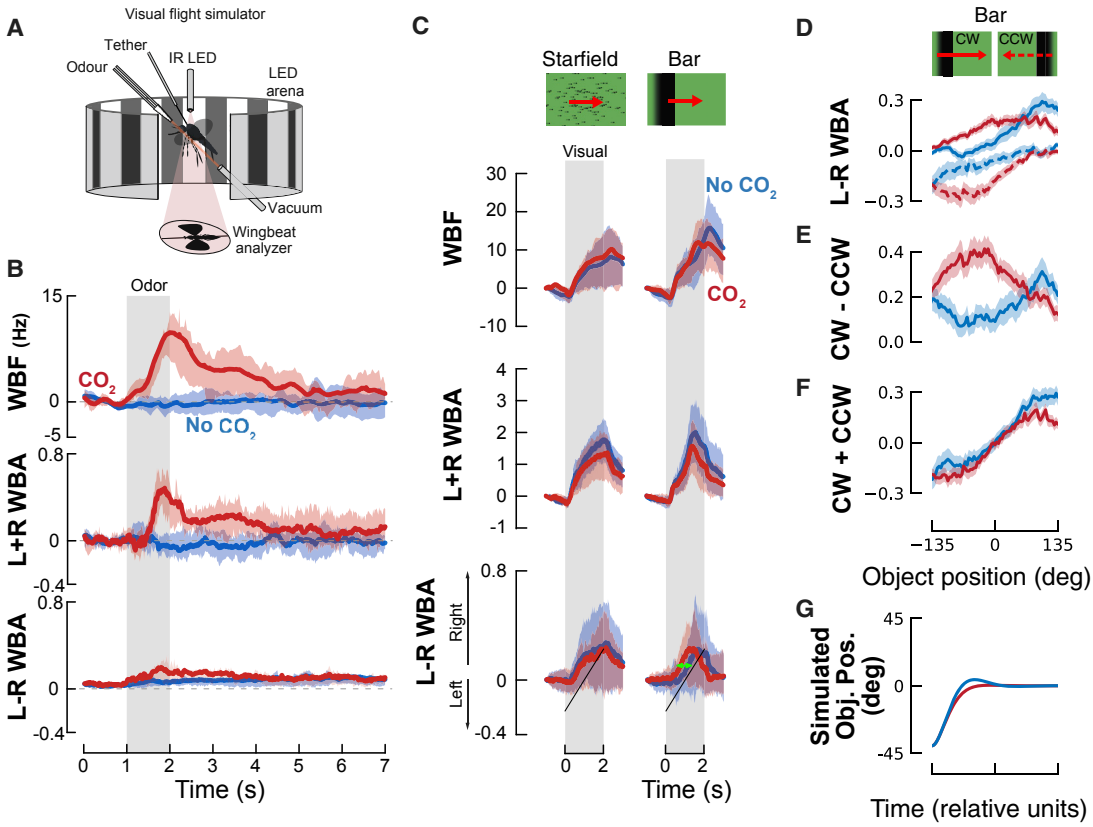

Figure 1. CO_2 Modulates Mosquitoes' Responses to Small-Field, Rotating Visual Objects

(A) Visual flight simulator (adapted from [18, 19]) used to record wing kinematics from a tethered mosquito.

(B) Stimulus-trigger-averaged changes in wingbeat frequency (ΔWBF), amplitude (L+R WBA), and steering (L−R WBA), in response to a 1-s pulse of 5% CO_2 (red solid lines) or a 1-s pulse of N_2 (no CO_2 condition, blue solid lines), indicated by the gray-shaded rectangle. Shaded areas represent the mean ± the first quartiles (n = 51).

(C) Mean responses of mosquitoes to a panel of visual stimuli (starfield yaw, 22.5° wide bars and squares). Top: normalized wingbeat frequency; middle: amplitude; and bottom: turning changes induced by the visual stimuli are shown. Turning responses correspond to average of the normalized responses to clockwise and counter-clockwise rotations. Plotted are the mean responses to visual stimuli in the absence (blue lines) and presence (red lines) of CO_2. Shaded areas denote the first and last quartiles around the mean (n = 86). Green arrow highlights change in dynamics that is investigated in (D)–(G).

(D) Steering responses, L−R WBA, for clockwise (solid lines) and counter-clockwise (dashed lines) moving bars and squares with CO_2 (red) and without (blue). Figure S1F shows the time responses corresponding to each of these traces.

(E) Velocity-dependent response, $r(\psi)$, calculated as the difference between the clockwise (CW) and counter-clockwise (CCW) responses from (D). The CO_2 and control responses for the bar are significantly different; p = 0.007 (resampling test); see Figure S2.

(F) Position-dependent response, $D(\psi)$, calculated as the sum of the CW and CCW responses from (D). The CO_2 and control responses for the square are significantly different; p = 0.003 (resampling test); see Figure S2.

(G) Simulated closed-loop object position, calculated by integrating Equation 3 (see STAR Methods for details).

Related to Figures S1 and S2 and Table S1.

maneuvers. In our preparation, we found increases of WBF and L+R WBA and, to a lesser extent, L−R WBA. The concentration of CO_2 emitted by humans is ~4.5% [25], and we observed the strongest kinematic changes in the tethered mosquitoes at concentrations of 5%–10% (Figure S1). We also tested pulse durations from 0.5 to 20 s and found 1-s pulses to elicit robust transient changes in kinematics, with longer pulses resulting in more sustained changes (Table S1).

Carbon Dioxide Modulates Responses to Object Motion, but Not Translational Motion

Given the robust responses obtained with 1-s pulses at 5% CO_2, we chose this concentration and pulse duration to investigate the effect of CO_2 on the responses to visual stimuli. Previous studies by Kennedy and others have examined the visual responses of mosquitoes in both free and tethered flight preparations and established the attraction of mosquitoes to dark objects [17, 26–28]. However, the responses of tethered mosquitoes to other types of visual stimuli have not been systematically studied.

To characterize the effect of CO_2 on tethered mosquitoes' visual responses, we first used several translational visual stimuli (Figure S1E), including expanding and regressing objects and patterns of optic flow [29], presented under open-loop conditions. In both the presence and absence of CO_2, these open-loop visual stimuli elicited two general types of responses in WBF. Frontally expanding patterns, such as looming objects or vertical bars and starfields creating progressive optic flow, all

elicited increases in wingbeat frequency, whereas contracting patterns, such as regressive motion and shrinking objects, elicited small decreases. All of these visual patterns, regardless of whether they were expanding or contracting, elicited small increases in wingbeat amplitude (L+R WBA). None of these responses were significantly altered in the presence of CO_2 (Figure S1E).

We next examined responses to horizontally drifting patterns (e.g., bar and starfield, Figure 1C; square, Figures S1F and S2A). For all horizontally drifting visual patterns, the mosquitoes followed the motion direction in both the presence and absence of CO_2 (Figures 1C and S1F). This contrasts the behavior of *D. melanogaster*, which turn toward bars taller than ~25° and turn away from smaller objects (8°–25° in height) in the absence of odor [30]. *D. mojaviensis*, however, exhibits behavior similar to the mosquitoes [31].

CO_2 had little effect on the mosquito's response to the wide field starfield stimulus. However, CO_2 did elicit subtle differences in all three kinematic measures in response to the bar and square. A decrease in WBF caused by CO_2 occurred after the end of the odor and visual presentation, making it difficult to interpret its behavioral significance. The wingbeat amplitude sum and difference, however, show CO_2 modulated differences throughout the stimulus. In the next section, we use a model to analyze the differences in the wingbeat amplitudes in more detail.

Carbon Dioxide Increases Object Tracking Fidelity in Tethered Mosquitoes

In both the presence and absence of CO_2, mosquitoes turned in the direction of horizontally moving bars and squares (Figure S1F). However, the dynamics of their turning behavior are modulated by the odor (green arrow, Figure 1C). To quantify these changes in dynamics, we modeled their behavior using the approach originated by Reichardt and Poggio [32]. This method makes it possible to characterize the closed-loop behavior using data collected with more controlled open-loop experiments, in which the stimulus spans a range of object positions and speeds. In particular, the approach allows us to combine the L−R WBA time series data (Figure 1C) from experiments done with clockwise and counter-clockwise moving objects (Figure 1D) to calculate functions that describe the velocity- and position-dependent steering responses of the insect (Figures 1E and 1F, respectively). Details of the analysis can be found in the STAR Methods.

The key insight from this analysis is that, for the bar, CO_2 increases the magnitude of the mosquitoes' velocity-dependent steering responses (Figure 1E), whereas the position-dependent response is only slightly modified (see Figures S2F and S2G for statistics). This is equivalent to increasing the damping of their response to target motion, which stabilizes their tracking behavior. To illustrate what this means for closed-loop behavior, we ran a simulation using the differential equations from the Reichardt and Poggio model together with our data (Figure 1G). This simulation shows that CO_2 reduces the overshoot and settling time of the bar tracking response, producing better tracking fidelity. We also found that CO_2-induced changes in the dynamics of the mosquitoes' tracking behavior of a small square target (Figures S2A–S2F). The changes in their responses were more variable and the effect sizes were smaller, making it difficult to interpret the effects of CO_2 with confidence. Thus, for the rest of this paper, we will focus on the mosquitoes' responses to moving bars.

It is important to emphasize the challenges of relating the temporal dynamics of tethered animals to freely flying animals, because, when on the tether, there is no proprioceptive feedback and we are only able to measure a few of the kinematic variables that are involved in flight maneuvers. Thus, our conclusion from these experiments is simply that CO_2 changes the dynamics with which mosquitoes track discrete objects, such as a bar, and these changes are generally consistent with their free-flight behavior. These results, however, allow us to begin searching for the neural basis of this modulation.

Odor Selectively Modulates Optic Lobe Responses

Given how odor stimuli modified steering responses to moving visual objects, we took the first steps toward localizing where in the brain this integration takes place by monitoring neural activity in the antennal lobe, a primary olfactory processing center, and the lobula, a 3rd-order neuropil in the mosquito optic lobe. We imaged calcium levels in groups of neurons with two-photon excitation microscopy (Figures 2A, 3A, and 3H) in an *Ae. aegypti* line (*PUb-GCaMP6s*) that expresses a genetically encoded Ca^{2+} indicator under the control of a ubiquitin promotor. Although this line does not permit cell-type-specific targeting, *PUb-GCaMP6s* is expressed strongly in axons and neuropil in the CNS and shows clear stimulus-evoked responses in the visual and olfactory brain regions (Figures 2 and 3) [35]. After image alignment and filtering (Figures 2A and 2B), we manually selected regions of interest (ROIs) that exhibited strong GCaMP6s expression. The ROIs we chose appeared to represent small bundles of axon terminals or dendrites, and we limited their size (40–100 μm^2) to prevent recording from large numbers of cells (see STAR Methods for details). After experiments, optical sectioning allowed 3D reconstructions of the imaged neuropil (Figures 2C, 3A, and 3H).

We focused on the lobula, because this area contains object-selective neurons in other dipteran species [36–39]. As a first step to characterizing responses within the lobula, we presented mosquitoes with a single moving bar, square (15°), or starfield pattern. We imaged 59 ROIs across 6 individual mosquitoes, and each stimulus type was presented 9 times. For each ROI, we compared the mean fluorescence during the first 2 s of visual motion to the mean fluorescence 2 s prior to the stimulus onset and compared these two datasets to a null distribution of 10,000 bootstrapped pairwise differences drawn from the combined datasets. Results from these analyses revealed that the moving bar evoked strong and significant responses in approximately 67% of the ROIs (Figures 2D and 2E). Consistent with our behavioral experiments, moving squares and wide-field motion of a starfield elicited less robust responses (28% and 13% of ROIs, respectively; Figures 2F, 2G, S3A, and S3B).

To examine how odor modulates the visually evoked responses in these ROIs (Figure 3A), we presented the mosquito with a moving bar, with and without CO_2 pulses, prior to the onset of the visual stimulus (Figures 3A and 3B). Similar to the above analysis, for each ROI, we assessed the difference between the odor and no-odor responses by comparing the data

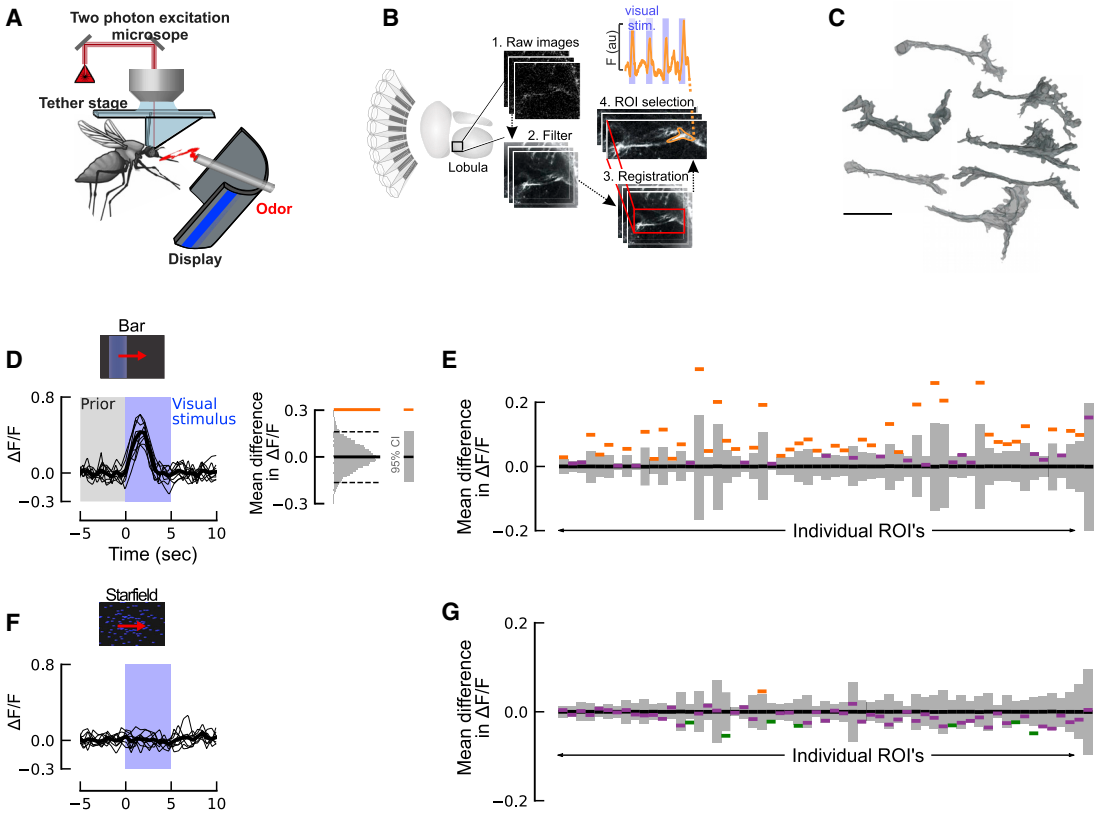

Figure 2. Lobula Responses to Visual Stimuli

(A) Schematic of the two-photon setup used to record calcium dynamics in the mosquito antennal and optic lobes.

(B) Diagram of the *Ae. aegypti* optic lobe, highlighting the lobula (left), and steps for ROI selection from the imaging plane: the raw images from the scanning plane are imported, and after image filtering and registration, ROIs are selected and the calcium dynamics are determined. Representative time trace of one lobula ROI from the filtered series shows stimulus-evoked responses to the visual stimulus (top trace; blue bars).

(C) Representative 3D reconstructions of ROIs that showed evoked responses to visual stimuli. Certain ROIs (right) showed tree-like dendritic branching, whereas others showed more columnar morphology (left). Although we were unable to assign imaged neuropil to orthologous neurons in other dipteran species, like *D. melanogaster*, intriguing similarities may exist based on their neuroanatomy, such as the lobula columnar (LC) or lobula tree-type (LT) cells [33, 34]. Scale bar, 20 μm.

(D) ΔF/F time trace for ROI no. 16, showing the strong response to the bar stimulus (left). Blue shading denotes time course of the visual (bar) stimulus, and gray shading denotes the prior baseline fluorescence that was used to calculate confidence intervals. To analyze the significance of the change in fluorescence of each ROI in response to a moving bar, we compared the mean fluorescence during the first 2 s of visual motion to the mean fluorescence 2 s prior to when the visual stimulus began (right). For both of these analyses, we calculated ΔF/F relative to the 5 s prior to the time of interest, which controls for slow changes in the fluorescence signal. For each ROI, the two datasets were compared to a null distribution of 10,000 bootstrapped pairwise differences drawn from the combined pre-visual stimulus and visual stimulus datasets. If the actual difference lies outside of 95% confidence interval (CI; gray bar) of this bootstrapped distribution, the difference is significant ($p \leq 0.05$; depicted by orange or green line).

(E) Confidence intervals based on null distribution of the baseline fluorescence before stimulation (gray bars); orange lines represent the responses of ROIs that are significantly greater ($p < 0.05$) than the null distribution; purple lines represent those ROI responses that are not significantly different from the null distribution ($p > 0.05$). Two-thirds of the ROIs we imaged in the lobula significantly responded to motion of a moving bar.

(F) Same ROI as (D) but in response to a moving starfield (blue shading denotes time course of the starfield stimulus).

(G) Same as (E) but for a moving starfield. Only 13% of the ROIs showed significant responses to the moving square ($p < 0.05$). Green lines represent the responses of ROIs that are significantly less ($p < 0.05$) than the null distribution (gray bars).

Related to Figure S3 and Video S1.

to a bootstrapped distribution of the combined odor and no-odor datasets (Figures 3B and 3C). In 14 of the ROIs (23%, including data from 5 out of 6 individuals; Figure S3C), the visually evoked responses were significantly larger ($p < 0.05$) when preceded by CO_2 (Figure 3D). On average, the relative increase in fluorescence for these modulated ROIs was 0.037, a 47% increase (Figures 3E–3G; Video S1). In 2 of the ROIs (3%), the responses were significantly smaller ($p < 0.05$; Figures 3E–3G). Note that, at a cutoff of $p = 0.05$, we would only expect 3 ROIs to exhibit a significant difference by chance, suggesting that most of the 16 ROIs that exhibited different visual responses are indeed being modulated by the preceding odor.

When a 2-s pulse of odor was presented without an accompanying visual stimulus, we found that the 14 positively modulated ROIs responded with an increase in fluorescence of 0.015 (Figure S3D). This increase in fluorescence could explain 40%

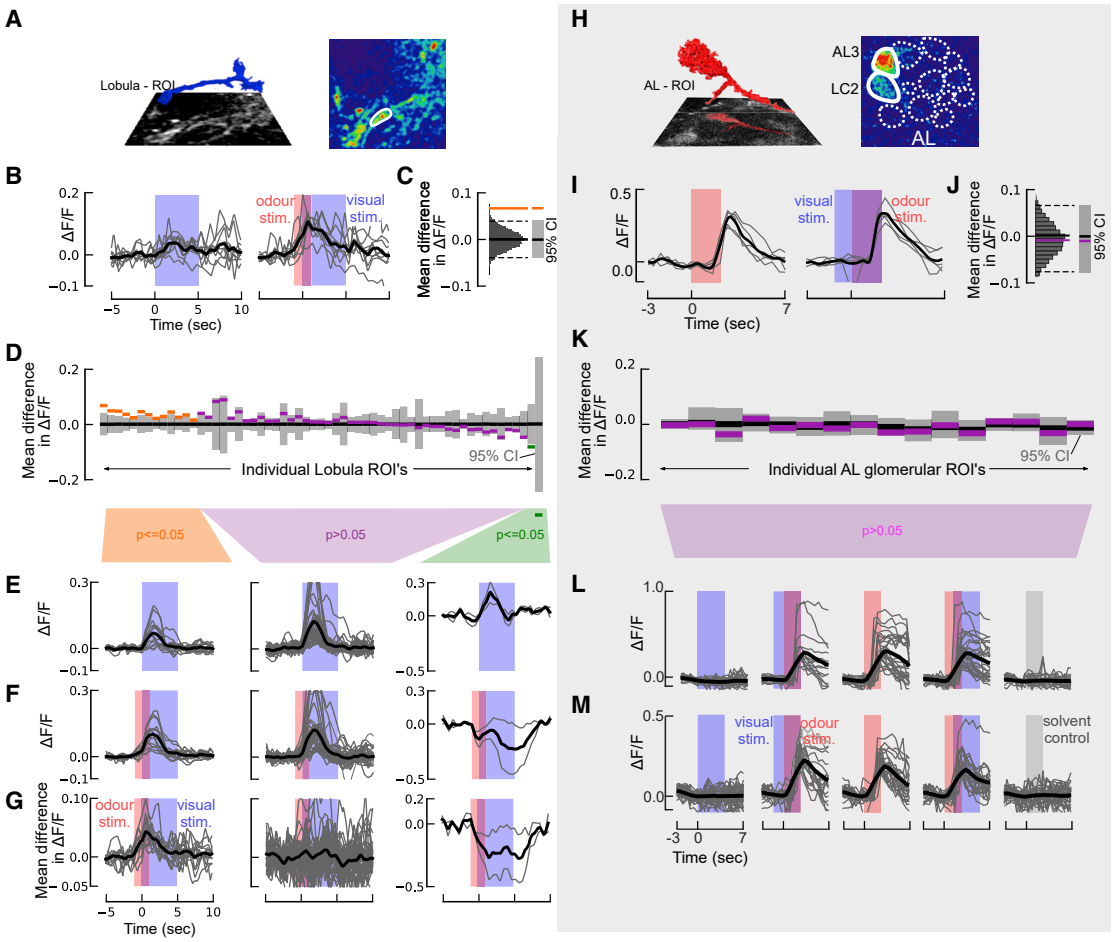

Figure 3. Calcium Imaging of Visual Responses in the Mosquito Antennal and Optic Lobes Reveals Asymmetric Neuromodulatory Effect of Odor

(A) 3D reconstruction of a lobula ROI inset above the imaging plane (left). Right: pseudocolor plot of the calcium fluorescence during the presentation of a visual stimulus is shown.

(B) Time series of ΔF/F in one ROI for 9 presentations of the visual stimulus (bar) without an odor stimulus (left; the visual stimulus is represented by the blue shading) and with an odor stimulus preceding and overlapping the visual stimulus (right; CO_2 stimulus is represented by the red shading). The maroon shading represents the time when the visual and odor stimuli overlap.

(C) To assess the difference in the response for the odor and no-odor experiments, we calculated the difference in the mean ΔF/F during the visual stimulus period for the two experiments (orange line). We then generated a null distribution by pooling the data from both experiments and bootstrapping 10,000 pairwise differences from this combined dataset (gray histogram). If the actual difference lies outside of 95% CI of this bootstrapped distribution (dashed lines), the difference is significant ($p \leq 0.05$; depicted by orange line).

(D) As in (C) but for the 59 lobula ROIs where the difference in mean ΔF/F for the odor and no-odor case, calculated as in (C). The results are plotted as in Figures 2E and 2G, and the ROIs in this figure are sorted in the same order shown in Figures 2E and 2G, allowing for a direct comparison.

(E) ΔF/F time traces for the "no odor" visual stimulus, split into the three statistical groups shown in (D). Thin traces show the average response for each ROI across 9 trials. Time course of the visual stimulus is represented by the blue shading.

(F) ΔF/F time trace for odor + visual stimulus experiments, as in (E). Blue and red bars denote the visual and CO_2 stimuli, respectively.

(G) Difference in the mean ΔF/F time traces shown in (E) and (F) for each ROI. Blue and red bars denote the visual and CO_2 stimuli, respectively.

(H) 3D reconstruction of the AL3 projection neuron (red) above the imaging plane (left) and (right) pseudocolor plot of the *Ae. aegypti* AL at the 30-μm imaging depth. AL glomeruli are depicted by dashed lines; the nonanal-responsive AL3 and LC2 glomeruli are depicted by the white solid lines.

(I) Time series of ΔF/F in one ROI for 5 odor stimulations without a visual stimulus (left; red shaded bar) and with a visual stimulus preceding the odor stimulus (right; blue bar represents the time course of the visual stimulus).

(J) As in (C) but for the AL3 glomerulus in (I).

(K) Difference in mean ΔF/F for the odor and odor + vision case for each of the 16 glomerular ROIs, calculated as in (C).

(L) ΔF/F time traces for the AL3 glomerulus in the different treatments: visual presentation alone (blue bar); visual presentation preceding the odor; odor alone (red bar); odor stimulus preceding the visual presentation; and no odor (mineral oil) control (gray bar). Thick trace (black) is the mean from 8 mosquitoes; thin gray traces are the individual stimulations across all animals (n = 4 or 5 per mosquito).

(M) As in (L) but for the LC2 glomerulus.

Related to Figure S3 and Video S1.

(0.015/0.037) of the odor-induced modulation of the visual response. ROIs that did not exhibit modulation of visual responses showed no response to the odor when presented alone, and ROIs that exhibited negative modulation also exhibited reduced fluorescence in response to the odor pulse (Figure S3D).

In conclusion, 67% of the 59 lobula ROIs we imaged exhibited significant responses to a moving bar, without any odor, and 23% of the ROIs exhibited a significant positive modulation of this visual response when the visual motion was preceded by a CO_2 pulse. These modulated ROIs also responded to a CO_2 pulse without any visual stimulus, but the magnitude of this olfactory response alone was less than half of the magnitude of the odor-induced change of the visual response. This suggests that the phenomenon is not simply a superposition of olfactory and visual responses but rather a super-linear, modulatory effect. Approximately 30% of the modulated ROIs only responded to the visual stimulus when it was preceded by a CO_2 pulse.

Visual Stimuli Do Not Modulate Responses in the Mosquito Antennal Lobe

If an odor can modulate the visual responses in the lobula, might visual stimuli have a similar effect on olfactory responses in the antennal lobe, perhaps via visual feedback from the mushroom bodies [40]? We conducted calcium imaging experiments on the olfactory glomeruli in eight animals using stimuli similar to those described in the previous section, in which an individual mosquito was presented with visual stimuli (moving bar) with and without pulses of CO_2 and nonanal, another host-emitted odorant [41]. Prior to odor stimulation, glomerular boundaries were discernible based on the baseline GCaMP6s expression, although significant calcium transients were not apparent. However, upon odor stimulation, the ventral antennal lobe (AL) glomeruli (AL3 and LC2), which are responsive to nonanal and other host odors, showed strong calcium responses that were time locked to the odor stimulus (Kruskal-Wallis test: $x^2 > 43.7$, $p < 0.0001$; multiple comparisons relative to control: $p < 0.001$; Figures 3H and 3I). When stimulated, dendritic arbors filling the AL3 and LC2 glomeruli and axons projecting into the coarse neuropil became observable (Figure 3H). When visual stimuli were presented with the odor—either 1 s before or 1 s after—we observed no difference in the response compared to when the odor was delivered alone ($p > 0.99$; Figures 3I–3M). Moreover, responses to isolated visual stimuli were not significantly different from the mineral oil (no odor) control ($p > 0.97$; Figures 3L and 3M).

Conclusions

Free-flight behavioral experiments with mosquitoes have shown that they integrate olfactory, visual, and thermal cues to function efficiently and robustly in complex environments [3]. In this current study, we took advantage of recent advances in genetic tools to probe where in the brain that integration occurs. These calcium-imaging methods, however, require that the animals be rigidly tethered to a head stage, which significantly alters sensory feedback. Furthermore, in these tethered preparations, we are only able to measure one of many parameters describing free-flight wing kinematics. This affects not only the behavioral readout but also our ability to provide realistic closed-loop virtual visual experiences. As a result of these limitations, it is difficult to directly compare the behavioral responses of tethered and freely flying animals. Despite these limitations, we were able to see significant effects of CO_2 on the behavior that are generally consistent with free-flight behavior, which allowed us to ask the question, ''where in the brain are olfactory and visual signals integrated in the mosquito?''.

Like mammals, insects exhibit symmetric sensory integration and modulation in higher order brain areas, such as the mushroom bodies [42–44] and central complex [45]. However, in contrast to mammals, insects also exhibit sensory integration and modulation in early sensory areas, such as in the antennal lobe [46] and optic lobe [47, 48]. Nonetheless, the degree to which sensory integration occurs in more peripheral processing areas for insects remains an open question. Our experiments suggest that, in *Ae. Aegypti*, sensory modulation is asymmetric: odor modulates vision, but not vice versa. Making a direct comparison between the two systems is difficult, as there are more regions and connections in the visual system compared to the olfactory system [33, 34, 49, 50]. Prior studies, however, suggest that an output region of the lobula, referred to as the optic glomeruli, shares many anatomical similarities with the antennal lobe [49], making these brain regions ideal for functional comparisons. Although we did not image from the optic glomeruli, the fact that we saw olfactory modulation in the lobula, one processing stage before the optic glomeruli, but no visual modulation in the antennal lobe suggests that the modulation is indeed asymmetric in these brain loci.

Why might sensory modulation in the mosquito be asymmetric? Insects, such as mosquitoes, have relatively poor visual resolution (5° compared to humans' 0.02°). Thus, for a mosquito, vision is unlikely to provide information about what something is. Instead, the odor may provide information for what the animal is smelling, and vision provides information for where the odor is located. These differences might explain the asymmetric sensory modulation we observed. Comparative studies across species with varying degrees of resolution in sensory modalities will be needed to address this hypothesis. Finally, there is a growing understanding of the molecular and neurophysiological bases of olfactory behaviors in mosquitoes [11, 13], but we know comparatively little about visual behaviors despite their importance for locating hosts and selection of biting sites [3, 51, 52]. Our results here provide motivation for addressing this research gap, as well as identifying the mechanisms by which olfactory input modulates other sensory systems. Fortunately, thanks to the recent development of new genetic tools, these types of experiments are now possible.

STAR★METHODS

Detailed methods are provided in the online version of this paper and include the following:

- KEY RESOURCES TABLE
- LEAD CONTACT AND MATERIALS AVAILABILITY
- EXPERIMENTAL MODEL AND SUBJECT DETAILS
- METHOD DETAILS
  - Tethered Flight Visual Arena
  - Odour delivery

SUPPLEMENTAL INFORMATION

Supplemental Information can be found online at https://doi.org/10.1016/j.cub.2019.06.043.

ACKNOWLEDGMENTS

Comments from three anonymous reviewers greatly improved the manuscript and analyses. We thank B. Nguyen for mosquito colony maintenance; J. Tuthill, A. Mamiya, and P. Weir for comments and help with the arena and imaging experiments; G. Wolff for comments and imaging assistance; and D. Alonso San Alberto for technical support. We acknowledge the support of the Air Force Office of Scientific Research under grants FA9550-14-1-0398 and FA9550-16-1-0167, NIH under grants 1RO1DCO13693 and 1R21AI137947, an Endowed Professorship for Excellence in Biology (J.A.R.), and the University of Washington Innovation Award. O.S.A. was supported in part by NIH grants 5K22AI113060 and 1R21AI123937.

AUTHOR CONTRIBUTIONS

C.V., F.V.B., A.L.F., M.H.D., and J.A.R. conceived the study. C.V., F.V.B., L.T.L., and K.K.S.T. participated in the execution and analysis of the arena assays. O.S.A. generated the GCaMP6 mosquitoes. J.A.R. conducted the imaging assays, and C.V., F.V.B., and J.A.R. analyzed the imaging data. C.V., F.V.B., and J.A.R. wrote the paper, and all authors edited the manuscript.

DECLARATION OF INTERESTS

The authors declare no competing interests.

Received: January 7, 2019
Revised: March 21, 2019
Accepted: June 13, 2019
Published: July 18, 2019

REFERENCES

1. Lehane, M.J. (2005). The Biology of Blood-Sucking in Insects (Cambridge University Press).
2. Turner, S.L., Li, N., Guda, T., Githure, J., Cardé, R.T., and Ray, A. (2011). Ultra-prolonged activation of CO2-sensing neurons disorients mosquitoes. Nature *474*, 87–91.
3. van Breugel, F., Riffell, J., Fairhall, A., and Dickinson, M.H. (2015). Mosquitoes use vision to associate odor plumes with thermal targets. Curr. Biol. *25*, 2123–2129.
4. McMeniman, C.J., Corfas, R.A., Matthews, B.J., Ritchie, S.A., and Vosshall, L.B. (2014). Multimodal integration of carbon dioxide and other sensory cues drives mosquito attraction to humans. Cell *156*, 1060–1071.
5. Gottfried, J.A., and Dolan, R.J. (2003). The nose smells what the eye sees: crossmodal visual facilitation of human olfactory perception. Neuron *39*, 375–386.
6. Gerber, B., and Smith, B.H. (1998). Visual modulation of olfactory learning in honeybees. J. Exp. Biol. *201*, 2213–2217.
7. Leonard, A.S., Dornhaus, A., and Papaj, D.R. (2011). Flowers help bees cope with uncertainty: signal detection and the function of floral complexity. J. Exp. Biol. *214*, 113–121.
8. Zhou, W., Jiang, Y., He, S., and Chen, D. (2010). Olfaction modulates visual perception in binocular rivalry. Curr. Biol. *20*, 1356–1358.
9. Cardé, R.T. (2015). Multi-cue integration: how female mosquitoes locate a human host. Curr. Biol. *25*, R793–R795.
10. Geier, M., Bosch, O.J., and Boeckh, J. (1999). Influence of odour plume structure on upwind flight of mosquitoes towards hosts. J. Exp. Biol. *202*, 1639–1648.
11. Zwiebel, L.J., and Takken, W. (2004). Olfactory regulation of mosquito-host interactions. Insect Biochem. Mol. Biol. *34*, 645–652.
12. Stanczyk, N.M., Mescher, M.C., and De Moraes, C.M. (2017). Effects of malaria infection on mosquito olfaction and behavior: extrapolating data to the field. Curr. Opin. Insect Sci. *20*, 7–12.
13. Lutz, E.K., Lahondère, C., Vinauger, C., and Riffell, J.A. (2017). Olfactory learning and chemical ecology of olfaction in disease vector mosquitoes: a life history perspective. Curr. Opin. Insect Sci. *20*, 75–83.
14. Corfas, R.A., and Vosshall, L.B. (2015). The cation channel TRPA1 tunes mosquito thermotaxis to host temperatures. eLife *4*, 1–10.
15. Zermoglio, P.F., Robuchon, E., Leonardi, M.S., Chandre, F., and Lazzari, C.R. (2017). What does heat tell a mosquito? Characterization of the orientation behaviour of *Aedes aegypti* towards heat sources. J. Insect Physiol. *100*, 9–14.
16. Muir, L.E., Thorne, M.J., and Kay, B.H. (1992). *Aedes aegypti* (Diptera: Culicidae) vision: spectral sensitivity and other perceptual parameters of the female eye. J. Med. Entomol. *29*, 278–281.
17. Kennedy, J.S. (1940). The visual responses of flying mosquitoes. Proc. Zool. Soc. London *A109*, 221–242.
18. Reiser, M.B., and Dickinson, M.H. (2008). A modular display system for insect behavioral neuroscience. J. Neurosci. Methods *167*, 127–139.
19. Frye, M.A., and Dickinson, M.H. (2004). Motor output reflects the linear superposition of visual and olfactory inputs in *Drosophila*. J. Exp. Biol. *207*, 123–131.
20. Gillies, M.T. (1980). The role of carbon dioxide in host-finding by mosquitoes (Diptera: Culicidae): a review. Bull. Entomol. Res. *70*, 525–532.
21. Chow, D.M., and Frye, M.A. (2008). Context-dependent olfactory enhancement of optomotor flight control in *Drosophila*. J. Exp. Biol. *211*, 2478–2485.
22. Fox, J.L., Aptekar, J.W., Zolotova, N.M., Shoemaker, P.A., and Frye, M.A. (2014). Figure-ground discrimination behavior in *Drosophila*. I. Spatial organization of wing-steering responses. J. Exp. Biol. *217*, 558–569.
23. Fox, J.L., and Frye, M.A. (2014). Figure-ground discrimination behavior in *Drosophila*. II. Visual influences on head movement behavior. J. Exp. Biol. *217*, 570–579.
24. Tammero, L.F., Frye, M.A., and Dickinson, M.H. (2004). Spatial organization of visuomotor reflexes in *Drosophila*. J. Exp. Biol. *207*, 113–122.
25. Dekker, T., and Cardé, R.T. (2011). Moment-to-moment flight manoeuvres of the female yellow fever mosquito (*Aedes aegypti* L.) in response to plumes of carbon dioxide and human skin odour. J. Exp. Biol. *214*, 3480–3494.
26. Ramachandra Rao, T. (1947). Visual responses of mosquitoes artificially rendered flightless. J. Exp. Biol. *24*, 64–78.
27. Bidlingmayer, W.L., and Hem, D.G. (1980). The range of visual attraction and the effect of competitive visual attractants upon mosquito (Diptera: Culicidae) flight. Bull. Entomol. Res. *70*, 321–342.
28. Bidlingmayer, W.L. (1994). How mosquitoes see traps: role of visual responses. J. Am. Mosq. Control Assoc. *10*, 272–279.
29. Weir, P.T., and Dickinson, M.H. (2015). Functional divisions for visual processing in the central brain of flying *Drosophila*. Proc. Natl. Acad. Sci. USA *112*, E5523–E5532.
30. Maimon, G., Straw, A.D., and Dickinson, M.H. (2008). A simple vision-based algorithm for decision making in flying *Drosophila*. Curr. Biol. *18*, 464–470.
31. Park, E.J., and Wasserman, S.M. (2018). Diversity of visuomotor reflexes in two *Drosophila* species. Curr. Biol. *28*, R865–R866.

32. Reichardt, W., and Poggio, T. (1976). Visual control of orientation behaviour in the fly. Part I. A quantitative analysis. Q. Rev. Biophys. *9*, 311–375, 428–438.
33. Otsuna, H., and Ito, K. (2006). Systematic analysis of the visual projection neurons of *Drosophila melanogaster*. I. Lobula-specific pathways. J. Comp. Neurol. *497*, 928–958.
34. Wu, M., Nern, A., Williamson, W.R., Morimoto, M.M., Reiser, M.B., Card, G.M., and Rubin, G.M. (2016). Visual projection neurons in the *Drosophila* lobula link feature detection to distinct behavioral programs. eLife *5*, e21022.
35. Bui, M., Shyong, J., Lutz, E.K., Yang, T., Li, M., Truong, K., Arvidson, R., Buchman, A., Riffell, J.A., and Akbari, O.S. (2018). Live calcium imaging of *Aedes aegypti* neuronal tissues reveals differential importance of chemosensory systems for life-history-specific foraging strategies. bioRxiv. https://doi.org/10.1101/345389.
36. Collett, T. (1971). Visual neurones for tracking moving targets. Nature *232*, 127–130.
37. Nordström, K., and O'Carroll, D.C. (2006). Small object detection neurons in female hoverflies. Proc. Biol. Sci. *273*, 1211–1216.
38. Nordström, K., Bolzon, D.M., and O'Carroll, D.C. (2011). Spatial facilitation by a high-performance dragonfly target-detecting neuron. Biol. Lett. *7*, 588–592.
39. Keleş, M.F., and Frye, M.A. (2017). Object-detecting neurons in *Drosophila*. Curr. Biol. *27*, 680–687.
40. Hu, A., Zhang, W., and Wang, Z. (2010). Functional feedback from mushroom bodies to antennal lobes in the *Drosophila* olfactory pathway. Proc. Natl. Acad. Sci. USA *107*, 10262–10267.
41. Syed, Z., and Leal, W.S. (2009). Acute olfactory response of *Culex* mosquitoes to a human- and bird-derived attractant. Proc. Natl. Acad. Sci. USA *106*, 18803–18808.
42. Gronenberg, W. (2001). Subdivisions of hymenopteran mushroom body calyces by their afferent supply. J. Comp. Neurol. *435*, 474–489.
43. Vogt, K., Aso, Y., Hige, T., Knapek, S., Ichinose, T., Friedrich, A.B., Turner, G.C., Rubin, G.M., and Tanimoto, H. (2016). Direct neural pathways convey distinct visual information to Drosophila mushroom bodies. eLife *5*, 14009.
44. Strube-Bloss, M.F., and Rössler, W. (2018). Multimodal integration and stimulus categorization in putative mushroom body output neurons of the honeybee. R. Soc. Open Sci. *5*, 171785.
45. Pfeiffer, K., and Homberg, U. (2014). Organization and functional roles of the central complex in the insect brain. Annu. Rev. Entomol. *59*, 165–184.
46. Nishino, H., Yamashita, S., Yamazaki, Y., Nishikawa, M., Yokohari, F., and Mizunami, M. (2003). Projection neurons originating from thermo- and hygrosensory glomeruli in the antennal lobe of the cockroach. J. Comp. Neurol. *455*, 40–55.
47. Suver, M.P., Mamiya, A., and Dickinson, M.H. (2012). Octopamine neurons mediate flight-induced modulation of visual processing in *Drosophila*. Curr. Biol. *22*, 2294–2302.
48. Maimon, G., Straw, A.D., and Dickinson, M.H. (2010). Active flight increases the gain of visual motion processing in *Drosophila*. Nat. Neurosci. *13*, 393–399.
49. Mu, L., Ito, K., Bacon, J.P., and Strausfeld, N.J. (2012). Optic glomeruli and their inputs in *Drosophila* share an organizational ground pattern with the antennal lobes. J. Neurosci. *32*, 6061–6071.
50. Fischbach, K.-F., and Dittrich, A.P.M. (1989). The optic lobe of *Drosophila melanogaster*. I. A Golgi analysis of wild-type structure. Cell Tissue Res. *258*, 441–475.
51. De Jong, R., and Knols, B.G.J. (1995). Selection of biting sites on man by two malaria mosquito species. Experientia *51*, 80–84.
52. Takken, W., and Verhulst, N.O. (2013). Host preferences of blood-feeding mosquitoes. Annu. Rev. Entomol. *58*, 433–453.
53. Trpis, M., McClelland, G.A., Gillett, J.D., Teesdale, C., and Rao, T.R. (1973). Diel periodicity in the landing of Aedes aegypti on man. Bull. World Health Organ. *48*, 623–629.
54. Vinauger, C., Lutz, E.K., and Riffell, J.A. (2014). Olfactory learning and memory in the disease vector mosquito *Aedes aegypti*. J. Exp. Biol. *217*, 2321–2330.
55. Klowden, M.J. (1995). Blood, sex, and the mosquito. BioScience *45*, 326–331.
56. Vinauger, C., Lahondère, C., Wolff, G.H., Locke, L.T., Liaw, J.E., Parrish, J.Z., Akbari, O.S., Dickinson, M.H., and Riffell, J.A. (2018). Modulation of host learning in *Aedes aegypti* mosquitoes. Curr. Biol. *28*, 333–344.e8.
57. Ignell, R., Dekker, T., Ghaninia, M., and Hansson, B.S. (2005). Neuronal architecture of the mosquito deutocerebrum. J. Comp. Neurol. *493*, 207–240.

STAR★METHODS

KEY RESOURCES TABLE

REAGENT or RESOURCE	SOURCE	IDENTIFIER
Antibodies		
GFP	Abcam	ab6556
Glutamine synthase	Sigma-Aldrich	MAB302
Biological Samples		
Heparinized bovine blood	Lampire Biological Laboratories	Bovine blood
Chemicals, Peptides, and Recombinant Proteins		
All odours for arena and imaging experiments	Sigma-Aldrich	N/A
Deposited Data		
Calcium imaging and behavioral data	This study	Mendeley Data (https://doi.org/10.17632/57pc9mkvft.1)
Experimental Models: Organisms/Strains		
Aedes aegypti Rockefeller strain	BEI	ROCK
Aedes aegypti GCaMP6s mutant strain	This study	GCaMP6 mutant
Software and Algorithms		
Kinefly	Custom	https://github.com/ssafarik/Kinefly
R	R Development Core Team	N/A
MATLAB	MathWorks	MATLAB and Statistics Toolbox Release 2012b, The MathWorks, Natick, Massachusetts, United States
ImageJ	NIH	https://imagej.nih.gov/ij/
Python (numpy, scipy, matplotlib)	Python Software Foundation and others.	http://www.python.org http://www.scipy.org/ http://www.numpy.org/ https://matplotlib.org/
Custom software	This study	J. Riffell (jriffell@uw.edu)
Other		
Wingbeat Analyzer	JFI Electronics / University of Chicago	N/A
Mosquito Electrophysiology Holder	This study	J. Riffell (jriffell@uw.edu)

LEAD CONTACT AND MATERIALS AVAILABILITY

Further information and requests for materials, resources and reagents, including mosquito lines, should be directed to and will be fulfilled by the Lead Contact, Jeff Riffell (jriffell@uw.edu).

EXPERIMENTAL MODEL AND SUBJECT DETAILS

Wild-type *Aedes aegypti* mosquitoes (line Rockefeller F25, MR4-735) were used for the tethered flight experiments. The colony was maintained in a climatic chamber at 25 ± 1°C, 60 ± 10% relative humidity (RH) and under a 12-12h light-dark cycle. An artificial feeder (D.E. Lillie Glassblowers, Atlanta, Georgia; 2.5 cm internal diameter) supplied with heparinized bovine blood (Lampire Biological Laboratories, Pipersville, PA, USA) placed on the top of the cage and heated at 37°C using a water-bath circulation, allowed us to feed mosquitoes on weekdays. Cotton balls soaked with 10% sucrose were continuously provided to the mosquitoes. Groups of 200 larvae were placed in 26x35x4cm covered pans containing tap water and were fed on fish food (Hikari Tropic 382 First Bites - Petco, San Diego, CA, USA). Groups of 120 pupae were then isolated in 16 Oz containers (Mosquito Breeder Jar, Bioquip Products, Rancho Dominguez, CA, USA) until emergence. Adults were then transferred into mating cages (BioQuip Products, Rancho Dominguez, CA, USA) and maintained on 10% sucrose.

Mosquitoes used in the calcium imaging experiments were from of the *Ae. aegypti* Liverpool strain, which was the source strain for the reference genome sequence. Briefly, this mosquito line was generated by injecting a construct that included the GCaMP6s plasmid (ID# 106868) cloned into the piggyBac plasmid pBac-3xP3-dsRed and using *Ae. aegypti* polyubiquitin (*PUb*) promoter fragment. Mosquito pre-blastoderm stage embryos were injected with a mixture of the GCaMP6s plasmid described above (200ng/μl) and a source of piggyBac transposase (phsp-Pbac, (200ng/μl)). Injected embryos were hatched in deoxygenated water and surviving adults were placed into cages and screened for expected fluorescent markers. Mosquitoes were backcrossed for five generations to our wild-type stock, and subsequently screened and selected for at least 20 generations to obtain a near homozygous line. The location and orientation of the insertion site was confirmed by PCR (see [35] for details).

To characterize the expression of GCaMP in different cell types in the AL, we double-stained for GFP (for the GCaMP6s; Abcam, Cambridge, MA, USA – Cat. no. ab6556; 1:1000 concentration) and glutamine synthase (GS; a glial marker; Sigma-Aldrich, St. Louis, MO, USA - Cat. no. MAB302; 1:500 concentration). Double-labeling of GFP (for GCaMP6s) and glutamine synthase (for glia) revealed that ubiquitous expression of GCaMP occurred in glia, local interneurons, and projection neurons. However, glia-like processes occurred on the exterior 'rind' of AL glomeruli and was restricted compared to the GFP labeling, thus enabling us to record from the central interior regions of the glomerular neuropil (Figure S3F). Similarly, GFP was strongly expressed in the optic lobe lamina and other loci, with restricted GS-labeling and little overlap (Figure S3F). In both brain regions, the GCaMP6s expression was very high in lobula cell types and AL projection neurons (PNs), such that during stimulation the cells could be imaged and tentatively reconstructed via optical sectioning.

For all the experiments, 6-8 day old female mosquitoes were used. For behavioral experiments, this gave mosquitoes the time to mate in the containers before the tethered flight experiments (random dissection of females revealed that 95% of them had oocytes); all experiments in the flight arena occurred during the last three hours of the mosquitoes' subjective day [52–55]. Female mosquitoes used in calcium imaging experiments were unmated and kept in isolation allowing fine-scale control of their age, reproductive status, physiological state, and sugar feeding. Previous studies have shown no differences between mated and unmated females in their host-seeking responses to odour cues [55]; as a first step we wanted to ensure that any neural modulation was due to the stimuli presented to the animals. Sugar feeding (10% sucrose) up to 16 h before experiments increased the calcium fluorescence and duration of the experiments.

METHOD DETAILS

Tethered Flight Visual Arena

Tethered flight responses by mosquitoes to olfactory and visual stimuli were tested in an LED-based arena (*sensu* [18]; Figure 1A). The arena consists of an array of 96 × 16 LEDs, each subtending 3.75° on the eye, subtending 360° horizontally and 54° vertically. Mosquitoes were cold anesthetized on ice and tethered to a tungsten wire using UV-activated glue (Loctite 3104 Light Cure Adhesive, Loctite, Düsseldorf, Germany) applied on the thorax. The main body axis was positioned at a 30° angle from the tether. Mosquitoes were then stored at room temperature in a closed container for an approximate 30 minute recovery period. Tethered mosquitoes were centered in a hovering position within the arena (Figure 1A [18]).

Mosquitoes were placed directly under an infrared (IR) diode and situated above an optical sensor coupled to a wingbeat analyzer (JFI Electronics, University of Chicago [18, 56]). The beating wings cast a shadow onto the sensor, allowing the analyzer to track the motion of both wings and measure the amplitude and frequency of each wingbeat. Measurements were sampled at 5 kHz and acquired with a National Instrument Acquisition board (BNC −2090A, National Instruments, Austin, Texas, USA).

Odour delivery

The mosquito was centered between an air inlet and a vacuum line aligned diagonally with one another, 30° from the vertical axis (Figure 1A). The air inlet was positioned 12 mm in front of and slightly above the mosquito's head, targeting the antennae from an angle of 15°. The vacuum line was positioned behind the mosquito 25 mm away from the tip of the abdomen. Two different airlines independently controlled by a solenoid valve (The Lee Company, Essex, CT, USA, LHDA0533115H) intersected this main air inlet, one delivering nitrogen and, the other, CO_2. Mass flow controllers for both the CO_2 and nitrogen delivery allowed for the CO_2 to be set at different concentrations (0, 1, 2.5, 5 and 10%) and pulse durations. Nonanal was diluted at 1:100 in mineral oil and 2 μL was pipetted on to a filter paper (2M Whatman) in a Pasteur pipette.

Mosquitoes responses to different CO_2 concentrations and pulse durations

For these experiments, a visual pattern of alternating vertical bars comprised of either inactive or fully-lit LEDs, each 16 × 6 pixels in size (i.e., 22.5° wide, 54° tall) was used. The pattern was briefly placed in closed-loop at the beginning of the experiment in order to encourage the mosquitoes to fly and then held motionless during the presentation of CO_2. Closed-loop control of the pattern position was achieved using the difference between the left and right amplitude signals. Concentrations of 5% and 10% CO_2 were initially tested, delivered for durations of 20, 10, 5, 1, and 0.5 s. One second pulses of CO_2 at 2.5% and 1% were also tested. Potential mechanical stimulation associated with the onset of the pulses was controlled for by delivering N_2 pulses for all the tested durations. Because a 1 s pulse of 5% CO2 was sufficient to produce a reliable, robust frequency response, this was the concentration and pulse duration used throughout the remainder of this study.

Moving visual patterns

To test the response to looming and drifting objects, large-field patterns of optic flow, and rotating field patterns, we adapted a broad panel of visual stimuli that are known to be important for guidance and stability during flight in other insects [29]: looming and fading squares, progressive and regressive bars, and starfield patterns (75% of pixels ON), yaw, a 22.5° wide square-like object (6 × 6 pixels, 20.25° tall) or a 22.5° wide and 54° tall bar moving either from left to right (Clockwise; CW) or from right to left (Counter-clockwise, CCW) (Figures 1 and S2). The stimuli were each presented for two seconds and were separated by a 4 s period during which all LEDs in the arena were lit. The angular velocity of objects moving on the display was 150°/sec. The entire experiment consisted of five trials of twelve visual stimuli presented twice (either immediately following a 1 s pulse of CO_2, or alone), the order of which was randomized at the beginning of each trial, using MATLAB's random number generator.

Dynamics model

To quantify the changes in visuomotor turning dynamics elicited by CO_2, we modeled their behavior using the approach described by Reichardt and Poggio [32]. Reichardt and Poggio describe the closed-loop behavior of a tethered insect steering toward an object with the following dynamics:

$$\Theta\ddot{\psi}(t) + k\dot{\psi}(t) = N(t) + S(t) - R(\psi(t), t), \quad \text{(Equation 1)}$$

where $\psi(t)$ is the angular position of the object on the mosquito's retina, Θ is the mosquito's moment of inertia, k is the aerodynamic friction, $N(t)$ is mean-zero Gaussian noise, $S(t)$ describes the motion of the object relative to stationary objects in the world, and $R(\psi(t), t)$ describes the mosquito's steering response. The steering response, $R(\psi(t), t)$, is a nonlinear function of the object's position and velocity on the retina, which may be approximated by [32]:

$$R(\psi(t), t) = r(\psi(t))\dot{\psi}(t) + D(\psi(t)), \quad \text{(Equation 2)}$$

where $r(\psi(t))\dot{\psi}(t)$ describes the mosquito's response to the velocity of the object, and $D(\psi(t))$ describes the mosquito's response to the position of the object.

The advantage of using open-loop data is that they provide information over the entire range of $\psi = [-\pi, \pi]$. These data can then be used to estimate $r(\psi(t))$ and $D(\psi(t))$ by comparing the mosquito's turning responses (L-R WBA) for objects moving in the clockwise (CW) and counter-clockwise (CCW) directions. The velocity component can be calculated from the difference, $r(\psi) = CW(\psi) - CCW(\psi)$ (Figure 1F), because the position components cancel out, whereas the position component can be calculated from the sum, $D(\psi) = CW(\psi) + CCW(\psi)$ (Figure 1G), because the velocity components cancel out [39]. The canonical shape for $r(\psi)$ is a positive even function, such as a horizontal line or cosine curve, and $D(\psi)$ is typically an odd function, such as a line with a positive slope or sine curve (corresponding to saturation at peripheral angles) [32]. These canonical shapes correspond to steering responses that are simultaneously proportional to the objects position and velocity.

In both the presence and absence of CO_2, mosquitoes' responses are proportional to the object's position and velocity, corresponding to object tracking. The precise shape of $D(\psi)$ and the magnitude of $r(\psi)$, however, changes in the presence of CO_2. To characterize these changes, we modeled $r(\psi)$ as a cosine, and $D(\psi)$ as a sine curve (Figures S2F and S2G). The cosine approximation of $r(\psi)$ is not perfect, however, the changes in magnitude are appropriately reflected in the model. For the square, CO_2 had little effect on $r(\psi)$, whereas it significantly increased the frequency of $D(\psi)$ ($p = 0.003$), contracting the sinewave, which corresponds to an increase in the slope of the proportional response when ψ is in front of the animal. For the bar, CO_2 significantly increased the magnitude of $r(\psi)$ ($p = 0.007$), corresponding to an increase in the velocity dependent response, and modestly increased the frequency of $D(\psi)$ ($p = 0.06$).

How might these changes in open-loop responses relate to free flight behavior? To gain a better intuition for how the functions $r(\psi)$ and $D(\psi)$ shape the mosquito's behavior, we simplified the dynamical system to bring it into a standard form. If we consider the mosquito interacting with a static object with some initial condition, we can eliminate $N(t)$ and $S(t)$ in Equation 1, since both are equal to zero, leaving us with the following nonlinear second order differential equation:

$$\Theta\ddot{\psi}(t) + (k + r(\psi(t)))\dot{\psi}(t) + D(\psi(t)) = 0. \quad \text{(Equation 3)}$$

We used cosine and sine approximations of $r(\psi)$ and $D(\psi)$ in Figure S3 to linearize the system about the stable equilibrium, $\psi = 0$, allowing us to approximate $r(\psi)$ as a constant, and $D(\psi)$ as a line, resulting in:

$$\Theta\ddot{\psi}(t) + (k + r_0)\dot{\psi}(t) + d_s\psi(t) = 0, \quad \text{(Equation 4)}$$

where $r_0 = r(\psi = 0)$ and d_s is the slope of $D(\psi)|_{\psi=0}$. This is a classic second order differential equation, equivalent to a mass-spring-damper system in which the slope of $D(\psi)$ determines the natural frequency and the magnitude of r_0 determines the damping. These parameters can be used to calculate how quickly the system responds to a step input, such as a mosquito seeing an object and steering toward or away from it. Larger values of d_s will reduce the response delay and increase the amount of oscillations, and larger values of r_0 will reduce the extent of any oscillations, thereby increasing the stability.

The results of our analysis suggest that CO_2 modulates flight behavior such that mosquitoes respond to visual objects with faster and more stable responses. To illustrate this, we numerically integrated Equation 3 using the sine and cosine curves from Figure S2 for $r(\psi)$ and $D(\psi)$ (Figure 1G) to simulate a mosquito turning toward a fixed object. Because the dynamics for tethered flight are slower

than free flight, and because of values for $r(\psi)$ and $D(\psi)$ are in relative units (based on the amplifier gains in the wing beat analyzer), we chose values for Θ and k to emphasize the relationship between $r(\psi)$ and the stability. The values we chose were $\Theta = 1$ (relative units) and $(\Theta/k = 3$ sec$)$. The ratio (Θ/k) represents the time constant of the passive rotational dynamics; values smaller than 1 ensure that the oscillations would be damped even with a small value for $r(\psi)$. The simulations show that CO_2 increases the speed of mosquitoes' responses to squares, at the expense of stability, and CO_2 dampens the oscillations of mosquitoes' responses to bars, increasing the stability at the expense of speed. Because the magnitude of the velocity response function was larger for bars (Figure 1F), and because this modulation increased the stability of the response, we chose to use bars as our primary visual stimulus for the calcium imaging.

Although it seems as though CO_2 has opposite effects on the dynamics for the bar and bar (compare Figures 1G and S2E), there are several explanations for this. First, the mosquitoes' behavior in response to the square was more variable, and the changes more subtle, thus the response may not be representative of their free behavior. Second, it is possible for one dynamical system to have opposite effects with an increase in gain depending on the initial gain. For example, when the system $G(s) = ((s+10)(s+0.5\pm1.5j))/((s+0.001)(s+0.5\pm0.5j))$ transitions from low to intermediate gain the stability decreases, but when it transitions from intermediate to high gain, the stability increases. If the mosquito's responses to bars and squares resulted in high and low initial gains, respectively, and the gain for each response increased multiplicatively due to CO_2, it would explain our results. However, we do not have sufficient data to test this hypothesis at present.

Calcium imaging

Image acquisition

Visual and odor-evoked responses were imaged in the lobula region of the mosquito optic lobe, and the antennal lobe region, taking advantage of our genetically-encoded ubiquitin-GCaMPs mosquito line [35] (Figures 2A–2C and 3H). Calcium-evoked responses were imaged using the Prairie Ultima IV multiphoton microscope (Prairie Technologies) and Ti-Sapphire laser (Chameleon Ultra; Coherent). The laser power was adjusted to 20mW at the rear aperture of the objective lens (Nikon NIR Apo, 40X water immersion lens, 0.8 NA), and bandpass filtered the GCaMP fluorescence with a HQ 525/50 m-2p emission filter (Chroma Technologies) and collected the photons using a multialkali photomultiplier tube. Images were collected at 2 Hz for each visual and visual+odour stimulus, for a total duration of 350 s (Figure 2), and calcium-evoked responses are calculated as the change in fluorescence and time-stamped and synced with the stimuli. Individual mosquitoes were tethered to a holder, and their cuticle removed to provide access to the antennal lobe or lobula regions of the brain [56]. The mosquitoes were placed at the center of a semi-cylindrical visual arena (frosted mylar, 20 cm diameter, 20 cm high); a video projector (Acer K132 WXGA DLP LED Projector, 600 Lumens) positioned in front of the arena projected the visual stimuli. To separate the wavelength of the light emitted by the projector from the GCaMP6 fluorescence, we used the projector's blue channel (peak at 451 nm, 18 lux, 0.02 W/m^2) and further reduced the longer wavelength component by covering the projector with three layers of blue gel filter (ROSCOLUX #59 Indigo). Select visual stimuli were the same as those used in the arena experiments: a bar, square (15°) and star-field pattern (comprising 75% of the screen).

Image analysis for Lobula ROIs

The ubiquitous expression of GCaMP6s made it difficult to distinguish between different cell types in the imaging planes. We thus used a series of criteria and image analyses to select ROIs manually. To ensure that mosquitoes were viable, we used animals that showed both odour-evoked changes glomerular fluorescence in the AL and changes in lobula fluorescence from stimulation with strong puffs of air to the head (via hand-held syringe) and from presentations of visual stimuli. Images were initially examined in ImageJ and imported into MATLAB for alignment using a single frame as the reference at a given imaging depth and subsequently registered to every frame to within ¼ pixel, and subsequently Gaussian filtered (2 × 2 pixel; σ = 1.5-3). For detection of the calcium dynamics, pixels were chosen based on fluorescence changes above the background threshold (1.02 to 15.9-times the baseline fluorescence), and ROIs were manually selected based on pixel intensities and appearances similar to axonal regions; restricted ROI surface areas (40-100 μm^2) were used to minimize recording multiple cells. Images were acquired at approximately 40 to 100 μm from the ventral surface (Figures 2 and 3) – neuropil in this region showed strong responses to visual stimuli, and odour-evoked modulation –, and optical sections (1 μm) were taken to tentatively reconstruct axonal regions associated with the regions of interest (Amira v.5, Thermo Fisher Scientific). We typically had stable imaging for approximately 1.5 h allowing complete testing of the experimental series.

Image analysis for AL ROIs

Antennal lobe ROIs were selected mainly based on the criteria listed above, except ROI selection was based on the clear delineation between glomerular boundaries. Glomerular ROIs were imaged at 40 μm from the ventral surface. Glomeruli at this depth show strong responses to either host- or plant-related odorants. For instance, the lateral cluster of glomeruli (AL3, LC2, V1) are especially responsive to host odorants, including nonanal, octanal, and hexanoic acid, and to a lesser extent, CO_2 (AL3, a glomerulus that is broadly responsive to stimuli), whereas glomeruli in the anteriomedial cluster respond to plant-related compounds, such as linalool, lilac aldehyde and myrtenol. At this depth, 14-18 glomeruli were neuroanatomically identified and registered between preparations. Calcium-evoked responses are calculated as the change in fluorescence and time-stamped and synced with the stimulus pulses. After an experiment, the AL was serially scanned at 1 μm depths from the ventral to the dorsal surface to provide glomerular registration to our tentative AL atlas (n = 6 female mosquitoes) as well as one that was previously published [57]. We note that glomeruli identified in our imaging experiments did not always conform, regarding glomerular number and position, to the previously published atlas; however, the two atlases provide a first principles approach for identifying and registering glomeruli.

QUANTIFICATION AND STATISTICAL ANALYSIS

Analyses were performed in R. For each stimulus, a baseline wingbeat frequency was determined by averaging the frequency across a 1 s time window preceding the stimulus delivery (either visual or olfactory, according to the experiment) and then subtracting this value from the max frequency values following the stimulus. Trials were discarded in which the mosquitoes stopped flying, indicated by a drop in wingbeat frequency below 200 Hz. The mean response for each individual was calculated from the saved trials and used as a replicate to calculate the mean response for each treatment group. This latter was calculated using the difference in frequency, turning tendency (L-R WBA), and total amplitude (L+R WBA) before and after the stimulus. One-tailed Student's t tests for paired samples were used to test for differences from baseline and t tests for independent samples were used to test for differences between groups. As stimuli that were presented with two directions of movement (i.e., square, bar and yaw from left to right or from right to left) did not elicit significantly different responses (Student t test; $0.06 < t > 1.15$; $40 < df < 84$; $p > 0.21$ for all comparisons), both directions of rotations were combined for the analysis. ANOVA and Tukey post hoc tests were employed for multiple comparisons. When specified, multiple pairwise t tests with Holm corrections were used to compare responses to visual stimuli. Whenever samples did not meet the normality assumption of the t test, a Wilcoxon test was performed. The delay before return to baseline wingbeat frequency was determined by determining the time at which the frequency signal crossed a threshold set at ½ standard deviation above the baseline mean frequency. The correlation between the turning response of the mosquitoes and the position of moving visual objects (i.e., squares and bars), were quantified using Equations 1, 2, and 3 in the text, and compared statistically using a resampling test.

Calcium imaging data were extracted in Fiji/ImageJ and analyzed in MATLAB and python. The trigger-averaged $\Delta F/F$ were used for comparing responses to visual and odour stimuli. To statistically determine visual-evoked responses, for each ROI we assessed the difference in mean fluorescence between the time period during the visual stimulus presentation and the time period preceding the visual stimulus by comparing the two datasets to a null distribution of 10,000 bootstrapped pairwise differences drawn from the combined pre-visual stimulus and visual stimulus datasets. Similarly, for examining odour-evoked modulation, for each ROI we assessed the difference between the odour and no-odour responses by comparing the difference in the mean fluorescence during the visual stimulus for these two experiments to a null distribution of 10,000 bootstrapped pairwise differences drawn from the combined odour and no-odour datasets.

Steering responses (e.g., Figures 1, S1, and S2) were compared using a resampling test, written in Python. For these tests we generated an exact null distribution by combining the CO_2 and control datasets, and randomly chose two samples (equal in size to the original datasets) from this combined dataset, fit sine and cosine curves to these samples, and compared the frequency and amplitude. We repeated this process 300 times to generate the null distributions shown in Figure S2. Then, we compared the actual difference in frequency and amplitude for the sine and cosine curves corresponding to the CO_2 and control trials, and compared these actual differences to the null distribution. This comparison provided a two-tailed p value indicating how likely the difference in these datasets was due to random sampling error.

DATA AND CODE AVAILABILITY

The behavioral and calcium imaging data generated during this study are available at Mendeley Data (https://doi.org/10.17632/57pc9mkvft.1). Code is available upon request.

Current Biology, Volume *29*

Supplemental Information

Visual-Olfactory Integration in the Human Disease Vector Mosquito *Aedes aegypti*

Clément Vinauger, Floris Van Breugel, Lauren T. Locke, Kennedy K.S. Tobin, Michael H. Dickinson, Adrienne L. Fairhall, Omar S. Akbari, and Jeffrey A. Riffell

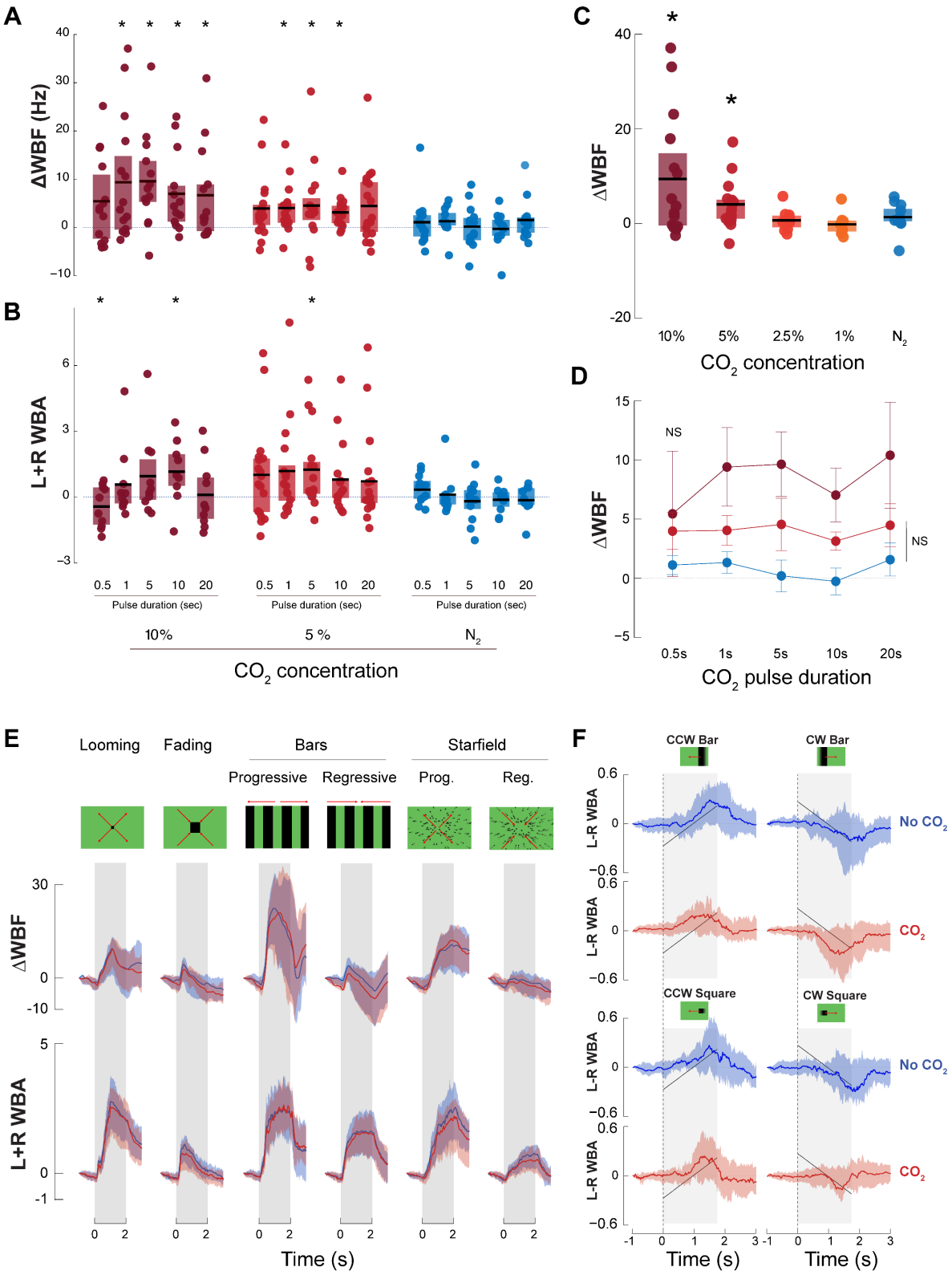

Figure S1. The effect of CO_2 duration and concentration and presentation of visual stimulus types on mosquito tethered flight kinematics (Related to Figure 1).

(A) Change in wingbeat frequency in the LED arena, after stimulation by CO_2 at different concentrations (10%, 5%, No-CO_2) and for various pulse durations (0.5-20s). Example schematics of ΔWBF and latency determination.
(B) Change in wingbeat amplitude after stimulation by CO_2 at different concentrations (10%, 5%, No-CO_2) and for various pulse durations (0.5-20s).
(C) Mean (±first and third quartiles) change in wingbeat frequency (ΔWBF) in response to pulses of CO_2 at different concentrations (0 to 10%). Asterisks denote significantly elevated responses with respect to the N_2 control ($p<0.05$; $n = 15$).
(D) Mean (±first and third quartiles) change in wingbeat frequency (ΔWBF) in response to pulses of 10% (dark red), 5% (red) CO_2 and N_2 (blue) of different durations.
(E) Mean responses of mosquitoes to a panel of visual stimuli. *Top*: normalized wingbeat frequency (ΔWBF), and *bottom*: amplitude (ΔWBA) changes induced by the visual stimuli. Plotted are the mean responses to visual stimuli in the absence (blue lines) and presence (red lines) of CO_2. Shaded areas denote the first and last quartiles around the mean. Grey bars indicate the presentation of the visual stimuli ($n = 86$).
(F) Mean (±first and third quartiles) responses to CCW and CW rotating bars and squares are represented with blue solid lines (No CO_2 condition) and red lines (CO_2 condition) ($n = 86$). Grey lines represent mosquito responses for each trial. Grey rectangles denote the presentation of the visual stimuli, and solid black lines the relative stimulus position. Positive stimulus positions indicate locations on the left, and vice versa, with 0° indicating that the stimulus was directly in front of the mosquitoes.

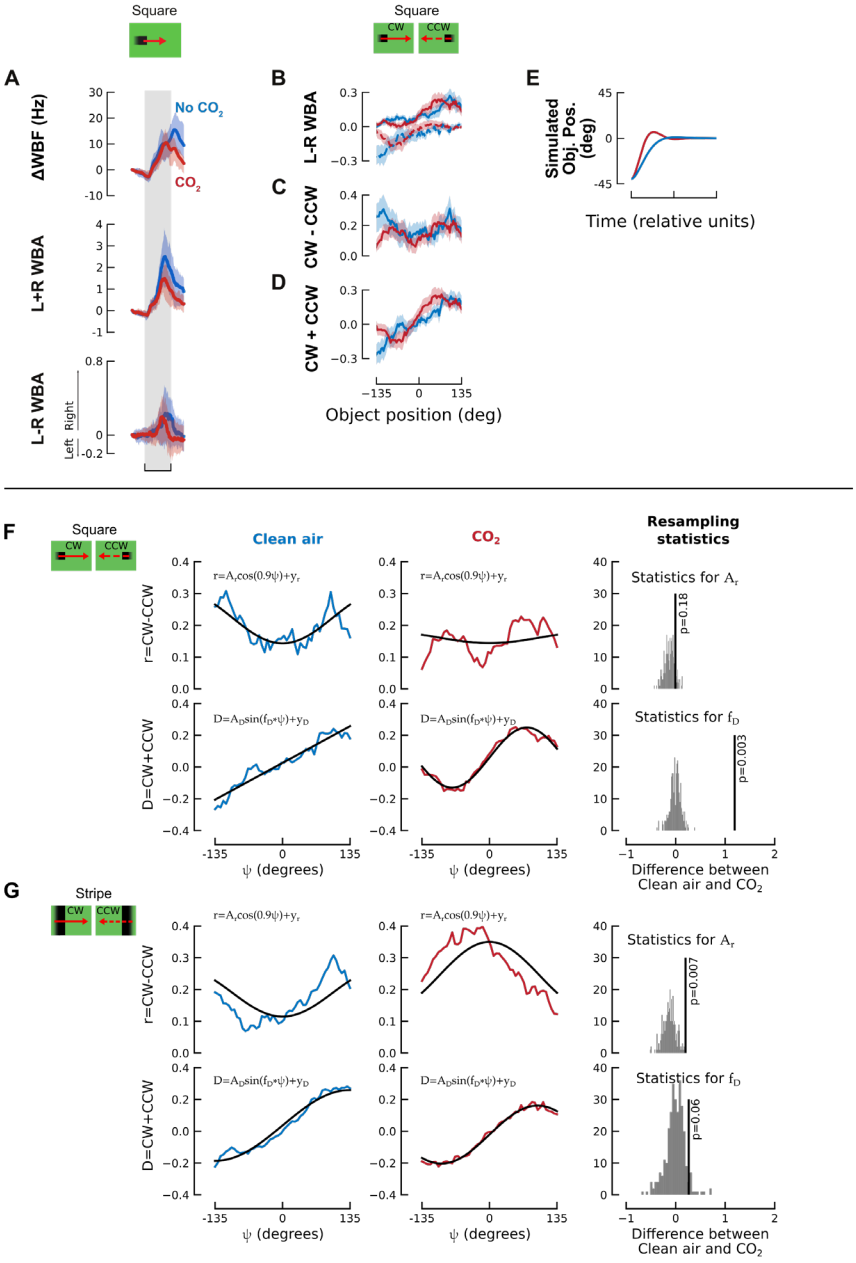

Figure S2. The effect of CO_2 and associated statistics related to mosquito responses to the presentation of the square and bar visual stimuli (Related to Figure 1).

(A-E) Data plotted as in Figure 1C-G, but for a square stimulus.

(F) *(left)* Velocity (r) and *(middle)* position (D) dependent functions from Figure 1E-F, with best-fit cosine and sine curves overlaid in black. For the sine curves, we fit the amplitude, frequency, and vertical offset using the scipy.optimize.fmin implementation of the downhill simplex algorithm. For the cosine curves we fit the amplitude and vertical offset; we omitted the frequency from the fit as it resulted in overfitting the noise. The key parameter for the D curve is the frequency, which determines the slope in the middle of the curve. The key parameter for the r curve is the amplitude, which determines the magnitude of the velocity response. *(right)* We determined the statistical significance of the difference between the clean air and CO2 experiments for these key parameters using resampling to construct a null distribution (300 resamplings), which we compared to the actual observed difference between these parameters.

(G) Same as F, but for a bar instead of a square (see panels A-E).

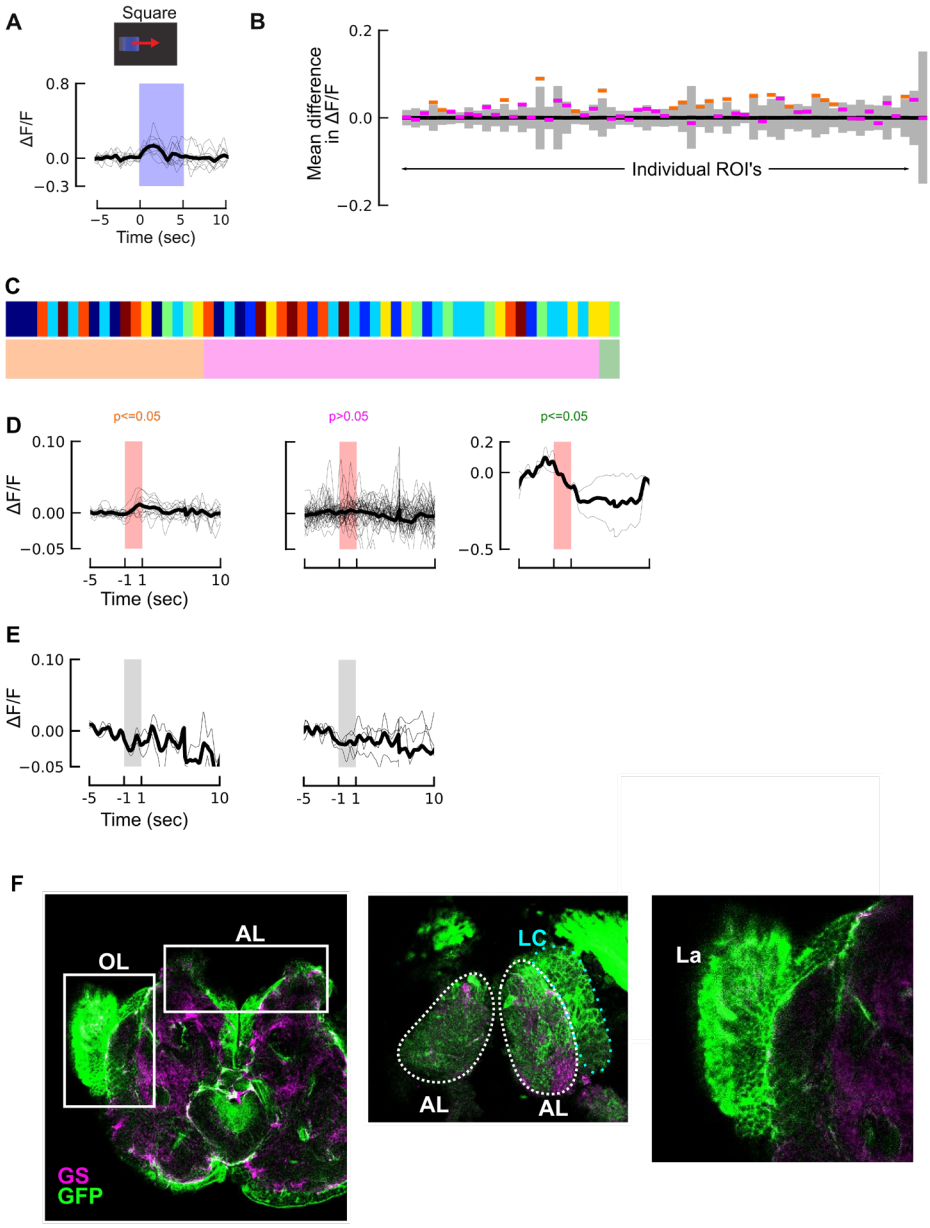

Figure S3. Lobula ROI responses to visual, odour, and mechanosensory stimuli, and associated expression of GFP and glutamate synthase in the mosquito brain (Related to Figures 2 and 3).

(A,B) Data plotted as in Figure 2D-E, but for a square stimulus. Only 13% of the ROIs showed significant responses to the moving square ($p<0.05$).

(C) Lobula ROIs ordered according to Figures 2 and 3 and coloured according to the preparation they were recorded from. The red, pink and green shaded areas immediately beneath denote the three statistical groups shown in Figure 3D.

(D) ΔF/F time traces for odour only experiments, split into the three statistical groups shown in Figure 3D. Lobula ROIs that showed significant modulation to the odour+visual stimulus also showed significant dynamics to the odour stimulus. The thick black lines denote the mean of individual ROI responses (grey lines).

(E) ΔF/F time traces for lobula ROIs that were stimulated with pulses of elevated air flow (grey bars). Previous research has shown that optic lobe neurons may be sensitive to sensorimotor feedback or mechanosensory input

[S1,S2]. We therefore tested elevated pulses of airflow (filtered air) comparable in magnitude to those used in our olfactory experiments. Both ROIs that were modulated by odour (*left*) and ROIs that were not modulated (*right*) showed no significant response to mechanosensory stimuli ($p>0.05$), suggesting that the mechanosensory component of the olfactory stimulus is not responsible for the modulation of visual responses in the lobula. However, more carefully targeted experiments will be needed to tease apart how odour and mechanical stimuli work together to modulate neuronal responses in the lobula. The thick black lines denote the mean of individual ROI responses (grey lines).

(F) Confocal images of brain sections from *PUb-GCaMP6s Ae. aegypti*. GFP immunofluorescence (green) reveals expression of GCaMP6s, which does not completely overlap with glia, labeled with antisera against glutamate synthase (GS, magenta). (*Left*) is the confocal image of the entire brain; boxes surround the AL or optic lobe (OL) loci. (*Right, top*) Staining of GS and GFP in the AL. The GS stains tend to show processes on the glomerular surfaces and along the rind of the glomeruli. By contrast, GFP staining shows fluorescence throughout the AL and glomerular neuropil. White dashed lines denote AL area; blue dashed line denotes lateral cell cluster (LC). (*Right, bottom*) In the optic lobe, GFP staining is strong in the lamina (La) and other optic lobe cell bodies and loci, whereas the GS staining is restricted to a few distinct cell bodies.

Two-way ANOVA

	Df	Sum Sq	Mean Sq	F value	Pr(>F)
duration	4	724	181.12	6.275	8.66e-05 ***
concentration	2	608	303.78	10.524	4.40e-05 ***
duration:concentration	8	239	29.84	1.034	0.412
Residuals	211	6091	28.87		

Signif. codes: 0 '***' 0.001 '**' 0.01 '*' 0.05 '.'

Table S1. Responses to CO_2 pulses are influenced by pulse duration and concentration (Related to Figure 1).

Supplemental References

S1. Suver, M.P., Mamiya, A. and Dickinson, M.H. (2012). Octopamine neurons mediate flight-induced modulation of visual processing in *Drosophila*. Curr. Biol., *22*, 2294–2302.

S2. Maimon, G., Straw, A.D. and Dickinson, M.H. (2010). Active flight increases the gain of visual motion processing in *Drosophila*. Nat. Neurosci., *13*, 393–399.